Environmental Science Nano

Theoretical Insight into the Adsorption of Aromatic Compounds on Graphene Oxide

Journal:	*Environmental Science: Nano*
Manuscript ID	EN-ART-04-2018-000384.R3
Article Type:	Paper
Date Submitted by the Author:	06-Aug-2018

Complete List of Authors:	Tang, Huan; Harbin Institute of Technology(HIT), Zhao, Ying; Harbin Institute of Technology, Shan, Sujie; State Key Laboratory of Urban Water Resource and Environment, Harbin 150090, China, School of Municipal and Environmental Engineering, Harbin Institute of Technology, Harbin 150090, China Yang, Xiaonan; a. State Key Laboratory of Urban Water Resource and Environment, Harbin 150090, China, b. School of Municipal and Environmental Engineering, Harbin Institute of Technology, Harbin 150090, China. Liu, Dongmei; Harbin Institute of Technology, Cui, Fuyi; Harbin Institute of Technology(HIT), State Key Laboratory of Urban Water Resource and Environment Xing, Baoshan; UMASS, Stockbridge School of Agriculture

Environmental significance statement

Aromatic compounds (ACs) and graphene oxide (GO) may be introduced into the water environment in their life cycles with their promising applications. Therefore, elucidating the interaction between GO and ACs will help to evaluate their environmental risks. In addition, a deep understanding of the interaction mechanism will allow the improvement for the decontamination and sensing of ACs with GO. Furthermore, the MD- and DFT-relevant measurements developed in this study will provide a platform to explore the behavior of other nanomaterials in water.

Environmental Science: Nano

ARTICLE

Theoretical Insight into the Adsorption of Aromatic Compounds on Graphene Oxide

Received 00th January 20xx,
Accepted 00th January 20xx

DOI: 10.1039/x0xx00000x

www.rsc.org/

Huan Tang [a,b,c], Ying Zhao [a,b], Sujie Shan [a,b], Xiaonan Yang [a,b], Dongmei Liu [a,b], Fuyi Cui [d,*], and Baoshan Xing [c,*]

In this work, adsorption of aromatic compounds (ACs) on graphene oxide (GO) was systematically investigated. Bisphenol A, nitrobenzene, phenol, benzoic acid, and salicylic acid were employed as representatives of ACs. Experimental isotherm analysis indicated the order of adsorption capacity is nitrobenzene > BPA> phenol > salicylic acid > benzoic acid. To examine which mechanism (including π–π, hydrogen bonds, vdWs, and hydrophobic interaction) governs the adsorption capacity, π–stacking ability, hydrogen bonds interaction energy, polarizability, and the interaction intensity of ACs with water were examined using molecular dynamic simulations and density functional theory calculations. The results showed that adsorption capacity was mainly guided by the π-stacking ability of ACs. Hydrophobicity, GO-ACs hydrogen bond, van der Waals, and electrostatic interaction may contribute to the adsorption of ACs on GO, but are not important in regulating the adsorption capacity. Local configurations of ACs adsorbed on GO were captured, and two patterns for multilayer adsorption were observed. Further analysis suggested that upon adsorbing on GO, the translational motion of ACs in water will be suppressed; however, the solvent accessible surface area will be increased, which may increase the bio-accessibility of ACs.

Introduction

Aromatic compounds (ACs), with one or more benzene rings in their chemical structure, are present in a wide variety of products used in our daily life.[1] Due to their growing applications, ACs are detected in water effluents and drinking water.[2, 3] Some ACs are endocrine-disrupting chemicals and can affect the growth and reproduction of many species even at very low concentrations.[4] For example, bisphenol A (BPA) can act through a variety of physiological receptors, such as the receptors of genomic estrogen, membrane-bound estrogen, androgen, and thyroid hormone.[5] Once entering into the water environment, ACs may accumulate and transfer through food chains in the ecosystems, and affect animal and human health.[6] ACs have been reported to occur in some surface water; for instance, the concentration of BPA in some drinking water sources is part-per-trillion (ng L^{-1}) to part-per-billion (μg L^{-1}).[2] Environmental exposures to many phenols are documented worldwide and exposures can be quite high (> 1 μM of urine metabolites).[7] Therefore, the removal of ACs from contaminated wastewater is becoming an important issue in environmental pollution and wastewater treatment.

The decontamination of ACs can be accomplished by various techniques such as photocatalytic, molecular-imprinted, biodegradation, advanced oxidation, and adsorption approaches.[8-12] Among these methods, sorption is one of the most widely used technologies considering its simple operation, low cost, and high efficiency. Recently, graphene-based nanomaterials have been used widely as adsorbent materials for ACs removal.[13-15] Graphene oxide (GO), a two-dimensional carbon-based material, has been extensively investigated to remove organic contaminants in environmental cleanup due to its large specific surface area and a variety of oxygenated functional groups.[16-18] Additional to the application for elimination of ACs, GO-based systems have been successfully employed for the electrochemical sensing of ACs.[19-21] In previous studies, the effect of solution chemistries (pH, ionic strength, and the presence of natural organic matter) and GO structural characteristics (wrinkles, folds, and grooves) were fully elucidated, and adsorption mechanisms were investigated employing adsorption isotherms and spectroscopic methods. π-π Interaction was verified to constitute one of the most important driving force governing the adsorption of ACs on GO.[16] However, quantitative measures to identify the π-π interaction intensity

[a] State Key Laboratory of Urban Water Resource and Environment, Harbin Institute of Technology, Harbin, 150090, China
[b] School of Environment, Harbin Institute of Technology, Harbin, 150090, China
[c] Stockbridge School of Agriculture, University of Massachusetts, Amherst, MA, 01003, USA
[d] College of Urban Construction and Environmental Engineering, Chongqing University, Chongqing, 40045,China
† e-mail: cuifuyi@hit.edu.cn, Tel: 86-13904503191 (Fuyi Cui).
e-mail: bx@umass.edu, Tel: 4135455212, (Baoshan Xing)

Electronic Supplementary Information (ESI) available: [Additional information regarding the preparing methods for GO, system setup for DFT calculations, parameters for adsorption isotherms, adsorption kinetic, LOLIPOP values of common aromatic compounds, and force field parameters]. See DOI: 10.1039/x0xx00000x

between GO and ACs is still scarce, and the configurations of ACs-GO after adsorption as a function of the concentration of ACs are unknown. Moreover, systematic studies and discussions on the mechanism that governs the adsorption capacity of GO towards ACs are still lacking. A thorough understanding of the interaction between GO and ACs will allow the improvement for sensing and removing ACs, thus, fundamental investigations are required.

To further address the interaction between ACs and GO, investigations with theoretical calculations should be conducted. Molecular dynamics (MD) simulation is a method allowing the physical movements of molecules to be characterized and giving a view of the dynamic evolution of the system.[22-24] Recent decades have seen tremendous efforts in exploring the adsorption mechanisms employing MD. Chen et al. captured the dynamic behaviour of pollutants on the surface of hexagonal boron nitride, and revealed the relationship between adsorption energies and n-octanol / water partition coefficient.[25] Tang et al. uncovered the mechanism behind the pH-dependent adsorption of ionizable compounds on GO using MD, and six kinds of hydrogen bond (H-bond) configurations during the adsorption process were observed.[26] Density functional theory (DFT) calculation has also proven to be an effective tool in probing the adsorption energy and configurations. Based on DFT theoretical calculations, Wang et al. examined the interaction mechanisms of organic compounds on graphene-related materials, and the computed results were further evidenced by experimental techniques.[27-30] Inspired by this, it is reasonable and important to explore the adsorption of ACs on GO combining experimental measurements, MD simulations, and DFT calculations.

Based on the above discussion, the adsorption of ACs on GO were explored systematically. BPA, nitrobenzene, phenol, benzoic acid, salicylic acid are widely used with considerable industrial importance and environmental impact, therefore, they were employed as representatives of ACs. Isotherm analysis was employed to explore the adsorption capacity of ACs on GO, and MD simulations and DFT calculations were performed to uncover the mechanisms behind the distinct adsorption capacity.

Experimental

Preparation and Characterization of GO

GO was synthesized through the reaction of graphite powder (Nanjing XFNANO Materials Tech Co., Ltd.) with $KMnO_4$ in a concentrated H_2SO_4 solution (the Hummers method).[31] Detailed preparation method is the same with our previous studies[32] and is provided in the Electronic Supplementary Information (ESI). Physical dimensions of GO were determined following an AFM procedure developed elsewhere.[33] X-ray photoelectron spectroscopy (XPS) and Fourier transform infrared spectroscopy (FTIR) were used to determine the surface functionalities of GO. The area under peaks from the XPS spectra was used for quantifying the relative concentrations of functional groups.

Adsorption Experiments

Adsorption experiments were conducted using a batch approach as reported in previous studies.[13] Adsorptions of ACs (0-500 mg/L) were carried out by mixing with GO (600 mg/L) in 10 mL vials at 25±1°C. The pH was adjusted to 7 by adding negligible volumes of 0.1 mol/L HCl or NaOH solution. The vials were placed on a shaker and agitated in the dark at 120 rpm for 24 h to reach an apparent equilibrium (preliminary experiments showed that there was no significant adsorption difference of ACs on GO after 24 h). After separation, the supernatant was immediately analyzed using high-performance liquid chromatography (HPLC).

Experimental data were obtained by the average values of triple parallel samples. The Langmuir and Freundlich models (eq 1 and 2) were used to fit the experimental isotherm data[34, 35]:

$$Q_e = \frac{q_m K_L C_e}{1+K_L C_e} \quad (1)$$

$$Q_e = K_F C_e^n \quad (2)$$

where C_e (mg/L) was the final concentration of ACs in aqueous solutions after sorption equilibration, Q_e (mg/g) was the amount of AC adsorbed on GO, q_m (mg/g) was the maximum sorption capacity, K_L (L/mol) was a constant that associated with the sorption energy, K_F [(mg/g)/(mg/L)^n)] was the Freundlich constant when the equilibrium concentrations of ACs reach to 1, and n represented the sorption intensity.

The kinetic data were fitted by pseudo-first order and pseudo-second-order models[27]:

$$\ln\left(q_e - q_{(t)}\right) = \ln q_e - k_1 t \quad (3)$$

$$\frac{t}{q_{(t)}} = \frac{t}{q_e} + \frac{1}{k_2 q_e^2} \quad (4)$$

where $q_{(t)}$ (mmol /g) was the amount of adsorbed ACs at time t (h), q_e (mmol /g) was the amount of adsorbed ACs at equilibrium, k_1 (1/h) and k_2 (mmol /(g·h)) were the rate constant of pseudo first-order and pseudo-second-order sorption, respectively.

MD simulation

GO used for MD simulation was built based on the Lerf-Klinowski model.[36] Carboxyl groups are attached to the carbon atoms on the edges. Epoxy and hydroxyl are the two dominant groups and are grafted to the carbon atoms on graphene basal plane. It is suggested that epoxy and hydroxyl are in proximity, moreover, the lowest-energy configuration is the one where the epoxy and hydroxyl are the nearest neighbours but located at the opposite sides of the graphene basal plane (Fig. 1(a)).[37] Electrophoretic mobility measurements indicated that GO is deprotonated and is negatively charged over the pH range from 1 to 12,[32, 38] therefore, half of the edge carboxyl groups are set to be deprotonated to mimic the property of GO in water and the model of GO was set to $C_{20}(\text{-O-})_2(OH)_2(COOH)_{0.5}(COO^-)_{0.5}$. The amount of deprotonated carboxyl groups in our model may different from the real situation in water environment, but will not affect the mechanism understanding, and similar models has been employed by other researchers and were proposed to perform well for exploring the properties of GO.[32, 39-41]. In the range of pH values usually observed

in the aquatic environment (5 to 9)[38], some ACs will be deprotonated. Therefore, the model of BPA, nitrobenzene, phenol, benzoic acid, and salicylic acid were built based on the pKa values (Table S1). The size of GO was 5.5 nm × 5.8 nm, and a ~ 13.0 × 13.0 × 13.0 nm^3 simulation box which contains ~ 80000 water molecules was used. 10 mM Na^+ and Cl^- were added to compensate for the net charges in the simulation box. Model of GO and detailed system setups are provided in Fig. 1.

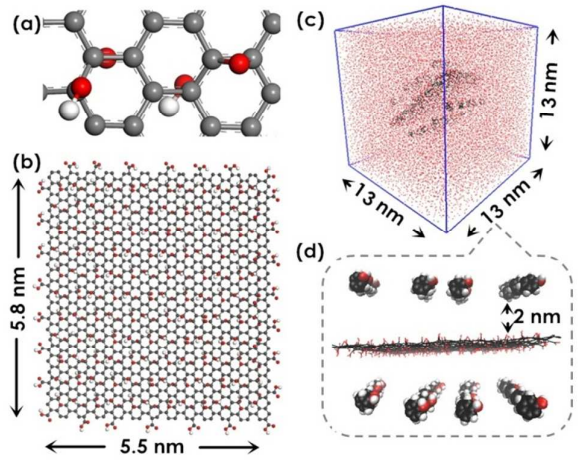

Fig. 1 Setup of the simulation system. (a) Positions of epoxy and hydroxyl groups on GO. (b) Model and dimension of the GO. (c) Dimension of the simulation system. (d) System setup for the adsorption of ACs on GO. The initial vertical distance between AC and GO is set at 2.0 nm. H in white, O in red, C in black, the tiny red dots represent water molecules, and the small molecules represent ACs.

The optimized potentials for the liquid simulations-all atoms (OPLS-AA) force field[42] implemented in the GROMACS software package[43] was used for simulating the adsorption of ACs on GO. The force field parameters were chosen accordingly with our previous studies and are given in ESI. Periodic boundary conditions were applied in all three directions. Water molecules were simulated using the standard SPC/E model.[44] Bond lengths were constrained with LINCS[45] and water geometries were constrained with SETTLE.[46] The cutoff for vdWs interaction was set to 1.0 nm. Before the MD began, energy minimizations were carried out. Then the systems were equilibrated for 100 ps at a temperature of 300 K (NVT) followed by a constant pressure of 1 bar (NPT). During the minimization and equilibration processes, the basal planes of the GO sheets and ACs were constrained. After annealing and equilibration, the simulated systems were run for 10-20 ns in an NVT ensemble at 300 K using a modified Berendsen thermostat[47]. The timestep was 2 fs and the trajectories were collected every 20 ps. Preliminary simulations showed that the simulation system will take ~5000 ps to reach equilibrium. Therefore, 10-20 ns are enough for our MD simulations. The system is considered to reaching an equilibrium when the fluctuations of temperature and total energy are within 10%. The MD trajectories resulting from the dynamic simulations were processed to extract structural and dynamical properties of the simulated systems. To identify the binding ability of ACs with water, the number of H-bonds forming between ACs and the surrounding water molecules was calculated. Specifically, we consider a bond to be an H-bond only if it meets the following two criteria: the donor-acceptor distance is smaller than 0.35 nm and the hydrogen donor acceptor angle is smaller than 30°.[43, 48] This criterion for H-bond has been used in previous studies.[39, 40, 49]

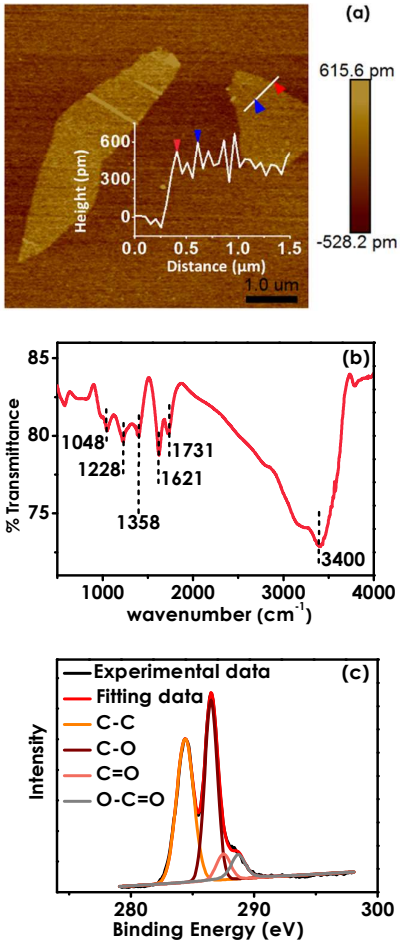

Fig. 2 Characterization of GO. (a) AFM image of GO. (b) FTIR spectrum of GO. (c) C 1s XPS spectrum of GO.

DFT Calculations

DFT Calculations were performed using Gaussian09 program.[50] Geometric optimizations for the calculations of interaction energy and LOLIPOP were performed using B3LYP functional with the 6-311+G** basis set, and DFT-D3(BJ) dispersion correction was employed. During the optimization, the whole system was free to move. Single point energies were calculated on the level of B3LYP/aug-cc-pVTZ. Polarizability was calculated on the level of PBE1PBE/aug-cc-pVTZ. Interaction energy (E_i) was calculated by the formula: $E_i = E_{[GO+AC]} - E_{[GO]} - E_{[AC]} + E_{BSSE}$, where $E_{[GO+AC]}$ represents

the total energy of the target GO-AC system, $E_{[GO]}$ is the total energy of GO, $E_{[AC]}$ is the total energy of AC, and E_{BSSE} is the basis set superposition error (BSSE) energy[51]. Because DFT calculations are time-consuming, smaller GO models (Fig. S1) were used and the system setups are provided in the ESI. LOLIPOP index was calculated using Multiwfn[52] to measure the π-stacking abilities of ACs.

PCM implicit solvent model was used. Note that the specific interactions that involve water cannot be described by implicit solvation, explicit water molecules were also included. To examine the H-bond interaction between ACs and water, 8 water molecules were placed around the ACs (Fig. S2). MD simulations showed the maximum amount of water molecules binding with ACs is 6, and therefore, 8 water molecules are enough for exploring the H-bond interaction. During the adsorption, there will be two kinds of H-bond interaction between ACs and the functional groups on GO: (1) H-bonds forming directly between ACs and the functional groups (ACs…GO); (2) water-bridged H-bonds forming between ACs and the functional groups (ACs…water…GO) through water. Therefore, two sets of DFT calculation systems were built (Fig. S3). For the water bridged H-bond, the amount of water in the "bridge" is not constant, and two molecules were used in our calculations.

Results and discussion

Characterization of GO

AFM image analysis confirmed that the GO sheets were single-layered and had plate-like structures (Fig. 2(a)). The thickness of GO was determined to be ~ 0.6 nm, consistent with the values reported in the literature.[38] The FTIR spectrum of GO is shown in Fig. 2(b). The large peak at approximately 3400 cm^{-1} is assigned to hydroxyl, which originates from water, hydroxide, and carboxyl groups. The sharp peaks at 1731, 1621, 1358, 1228, and 1048 cm^{-1} are assigned to C=O, aromatic C=C, carboxyl O=C-O, epoxy C-O, and alkoxy C-O bending motion, respectively. [53, 54] These functional groups were further analysed using the XPS. As shown in Fig. 2(c), the carbon existed mainly in four forms, that is, nonoxygenated C-C carbon (284.8 eV), carbon in C–O (286.5 eV), carbon in C=O (289.5 eV), and carbon in O=C–O (288.7 eV). The percentage of different functional groups in GO is calculated based on the XPS spectrum and is shown in Table S2.

Adsorption Capacity of ACs on GO

Sorption isotherms of ACs on GO are shown in Fig. 3, and the relative parameters calculated from the Freundlich and Langmuir models are provided in Table S3. The q_m values demonstrated that the adsorption of nitrobenzene on GO (263.24 mg/g) was the most favourable; BPA was the second favourable with a q_m value of 224.32 mg/g. By contrast, the adsorptions of phenol (56.56 mg/g), salicylic acid (33.64 mg/g), and benzoic acid (21.27 mg/g) on GO were not very significant. The adsorption capacity for nitrobenzene is similar with a previously reported value of 295.1 mg/g,[16] and the subtle difference may be due to the different compositions of GOs. The data for the other ACs used in this study are not found in the literature.

To uncover the mechanisms behind the different adsorption capacities, driving forces during the adsorption should be examined. The underlying mechanisms involved in the adsorption of organic compounds on GO include H-bond, π-π, van der Waals, electrostatic, and hydrophobic interactions. Therefore, MD simulations and DFT calculations were performed to identify the dominant force that governs the adsorption capacity of ACs on GO.

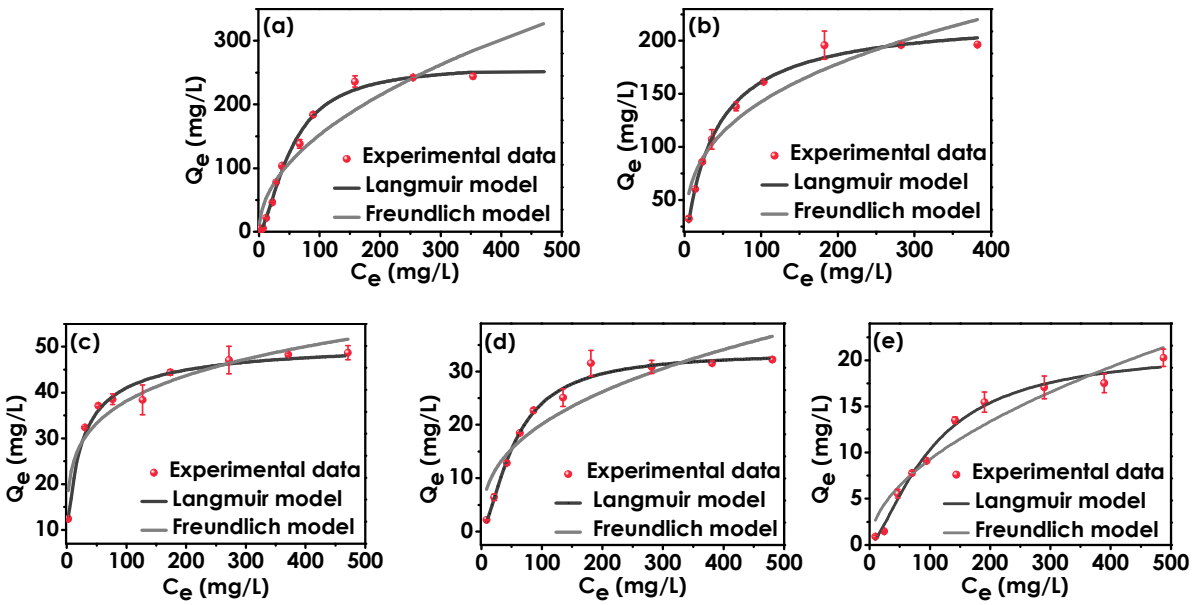

Fig. 3 Sorption isotherms of (a) nitrobenzene, (b)BPA, (c)phenol, (d) salicylic acid, and (e) benzoic acid on GO.

Hydrophobic Interaction

Hydrophobic interaction was suggested to be one of the most important adsorption mechanisms for hydrophobic and nonpolar ACs with the graphitic domains of GO. Octanol-water distribution coefficient and aqueous solubility of the AC molecules have been used to determine the intensity of the hydrophobic interactions.[55-57] These parameters are all related to the affinity between ACs and water. Along these lines, the ability of forming H-bond with water, which is an indicator for the intensity of binding with water, can also be employed to measure the hydrophobicity of ACs. The ability of forming H-bond with water can be obtained by calculating the amount of H-bond forming between ACs and water and the interaction energy of AC…water H-bond. For specifically, AC with stronger hydrophobicity will form less AC…water H-bond and possesses lower H-bond interaction energy. Based on the above discussions, MD simulations and DFT calculations were performed to examine the hydrophobicity of ACs. Considering that BPA possess two benzene rings and two hydroxyls, and to make the interaction intensity between ACs and water independent of the composition of ACs, the interaction energy and the amount of H-bond were divided by the relative molecular mass of AC, and the configurations of the AC-water H-bonds are shown in Fig S4.

The MD results agree well with the DFT results that the order of the hydrophobicity of ACs is (Fig. 4(a) and (b)): BPA >nitrobenzene > salicylic acid > benzoic acid > phenol. This order correlates poorly with the order of adsorption capacity (nitrobenzene > BPA > phenol > salicylic acid > benzoic acid), implying that the hydrophobicity of ACs is not an important factor that determines the adsorption capacity of ACs on GO. It should also be noticed that the order of aqueous solubility (phenol (83000 mg/L, 20 °C) > benzoic acid (3440 mg/L, 25 °C) > salicylic acid (2480 mg/L, 25 °C) > nitrobenzene (1900 mg/L, 20 °C) > BPA (1000 mg/L, 21.5 °C))correlated well with the ACs-water H-bond intensity, implying that the H-bond intensity is efficient in comparing the hydrophobicity of ACs.

Free energy of transfer between water and oil is also a way to quantify the ACs' hydrophobicity, and therefore, was calculated to examine whether it correlates well with the adsorption capacity. The free energy of transfer (E_f) was calculated on the level of M052X/6-31G* (scrf=SMD) by the formula: $E_f = E_{[water]} - E_{[n\text{-}hexadecane]}$, where $E_{[water]}$ and $E_{[n\text{-}hexadecane]}$ represents the solvation free energy of ACs in water and in n-hexadecane. In general, the more positive E_f is, the more hydrophobic the AC is. As shown in Table S4, the order of ACs' hydrophobicity indicated by E_f is: salicylic acid > nitrobenzene > benzoic acid > phenol > BPA. This order correlated poorly with the adsorption capacity of ACs on GO, indicating that the free energy of transfer is not efficient in predicting the adsorption capacity.

H-Bond Interaction

There are two kinds of H-bonds forming between ACs and the functional groups on GO during the adsorption: the direct ACs…GO H-bonds and the water-bridged ACs…water…GO H-bonds. Considering it is impossible to isolate the H-bond interaction energy from the total interaction energy (includes vdWs, H-bond, π-π, etc..), bond length and bond angle were employed to compare the H-bond interaction intensity. Based on the classification of Jerrey (Table S5)[58], H-bonds with shorter length and larger angle are considered as stronger H-bond interactions. As shown in Fig. 5 and Fig. S5, hydroxy, epoxy, and carboxyl interact the most strongly with benzoic acid, BPA, and phenol, respectively. This trend indicates that the direct H-bond between GO and ACs is not a dominant factor that determines the adsorption capacity.

The water-bridged ACs…water…GO H-bonds (Fig. 5 and Fig. S5) plays two distinct roles during the adsorption. On the one hand, this H-bond represents a minor driving force; for example (Fig. 5), there is no direct H-bond between nitrobenzene and the epoxy groups on GO, and one water molecule bridged GO and nitrobenzene by one moderate (2.03 Å, 149.697°) and one weak (2.23 Å,132.213°) H-bond. On the other hand, this kind of H-bond hinders the direct interaction between GO and ACs. More specifically (Fig. 5), in the absence of water, benzoic acid and the hydroxy form a strong direct H-bond (1.28 Å, 179.688 °); however, upon the formation of water bridged H-bond, this direct H-bond was impaired (1.52 Å, 172.404°). By comparing the water-bridged H-bond properties in Fig. S5, it is concluded that the water-bridged H-bond is not important in regulating the adsorption capacity.

To make it more convincing that the water-bridged H-bond exists during the adsorption process, MD trajectories were extracted and the water-bridged H-bonds were observed (Fig.S6). The detailed property of the water-mediated H-bond (bond length and bond angle) may be different from the DFT results. This is because the system setups for MD and DFT calculations are different: only two water molecules were employed, and the model of GO was simplified in DFT calculations; in MD simulations, the model of GO with many functional groups was large and was surrounded by ~ 80000 water molecules; therefore, different property of the water-bridged H-bond is reasonable.

In summary, the H-bond between GO and ACs is not a dominant factor that affects the adsorption capacity, and other driving forces should be further investigated. π-π Interaction was suggested to be important in influencing the adsorption preferences of ACs on GO.[59] Therefore, the π-stacking intensity between GO and different ACs was examined.

π-π Interaction

Bloom and Wheeler proposed that electrons confined to their atomic rings can deliver stronger π-stacking interactions than those being delocalized in aromatic systems.[60] Based on this proposal, Jérôme et al. introduced a quantitative criterion, namely the LOLIPOP (Localized Orbital Locator Integrated Pi Over Plane) index, to characterize the π-electronic nature of aromatic molecules and provide information regarding their π-stacking ability. They argued that benzene ring with smaller LOLIPOP value has stronger π-stacking ability, implying that strong π-π interaction was likely to occur for ACs with smaller LOLIPOP values. LOLIPOP values of the ACs are shown in Fig. 4(c). To make the π-stacking ability independent of the weight of ACs, the LOLIPOP values were divided by the relative molecular mass of ACs. By comparing the LOLIPOP values of each AC, it is clear that for BPA, phenol, salicylic acid, and benzoic acid, the order of the LOLIPOP value aggress well with the

order of the adsorption capacity. Therefore, π-π interaction is a major factor in regulating the adsorption capacity. It should also be noted that nitrobenzene exhibited the second weakest π-stacking ability and possessed the highest adsorption capacity, which implies that the π- π interaction itself may not completely explain the adsorption capacity of ACs on GO, and other driving forces should be further examined.

Considering there is no quantitative index for evaluating the π-stacking ability of common ACs, the LOLIPOP values of 20 kinds of ACs were calculated (Fig. S7). These LOLIPOP values will help to compare the π-π interaction intensity between ACs and materials containing benzene rings.

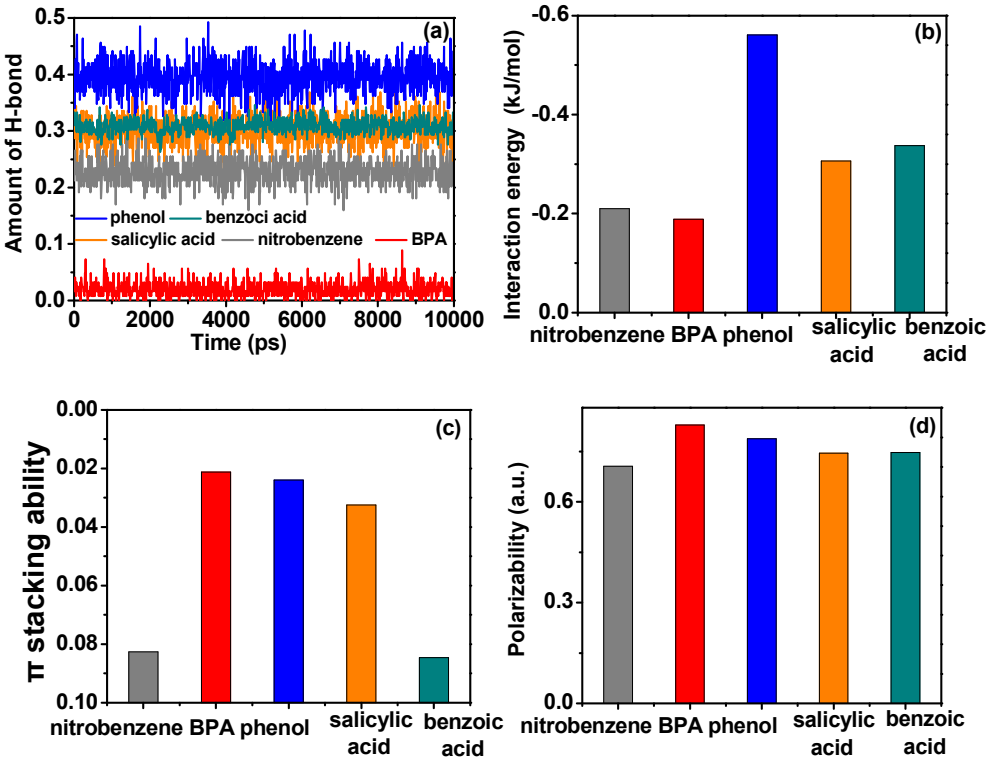

Fig.4 MD and DFT results for the interaction intensity of hydrophobic, π-π, and vdWs interactions (the values in the figures are all normalized by the molecular weight of ACs). (a) Amount ACs…water H-bonds. (b) Interaction energy of AC…water H-bond (c) LOLIPOP values of ACs. (d) Polarizabilities of ACs.

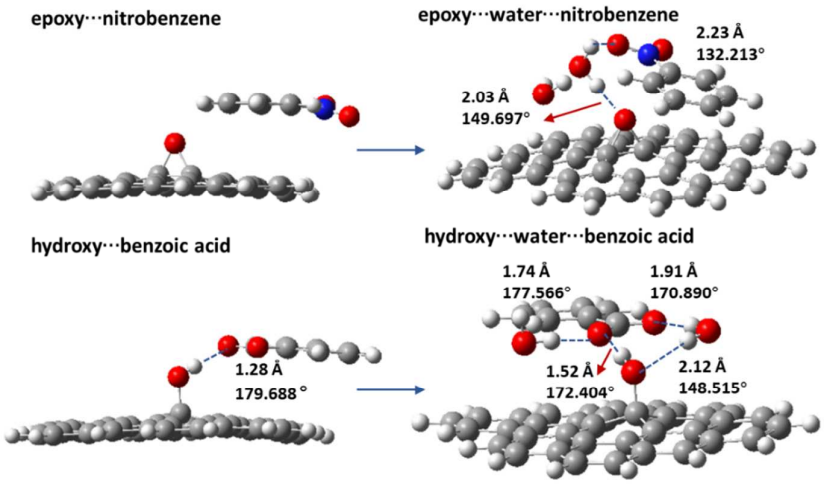

Fig 5. Direct H-bond and water-bridged H-bond

vdWs Interaction

The vdWs forces, also known as London forces, are weak interactions caused by momentary changes in electron density in molecules. The interaction includes either the attraction or repulsion between AC molecules and GO surface. Though vdWs interaction is weak, its long-range nature and collective effect can be important in the interactions between GO and ACs. vdWs interaction intensity is proportional to the polarizability.[61] To investigate whether the vdWs exert any effect on the adsorption capacity, polarizability of the ACs are calculated. As shown in Fig. 4(d), the highest polarizability is for BPA (0.83), phenol (0.79) and benzoic acid (0.75) are in the middle, and salicylic acid (0.74) and nitrobenzene (0.71) with the lowest values. Therefore, the vdWs interaction intensity between GO and ACs is BPA > phenol > benzoic acid > salicylic acid > nitrobenzene. Notably, this order correlated poorly with the adsorption capacity among the five adsorbates, implying that the vdWs interaction is not a crucial factor controlling the adsorption capacity.

Electrostatic Interaction

The presence of charged functional groups on ACs and GO indicates that electrostatic interaction may be important in regulating the adsorption capacity. The pKa values of GO are 4.3, 6.6, and 9.8, with 4.3 and 6.6 corresponding to the ionization of the carboxylic group, and 9.8 corresponding to the ionization of the hydroxyl group.[62] The pK_a of BPA, phenol, benzoic acid, and salicylic acid is 9.0, 9.9, 2.98, and 4.2, respectively. [63, 64] The range of pH usually observed in the aquatic environment is from 5 to 9,[38] implying that GO, BPA, benzoic acid, and salicylic acid will be deprotonated. Upon the ionization, GO and ACs are negatively charged and there will be electrostatic repulsion between GO and ACs. Nitrobenzene is neutral and is free of the electrostatic repulsion during adsorption, indicating that the zero-electrostatic repulsion also contributes to the higher adsorption capacity of nitrobenzene. However, comparing phenol with BPA yields the conclusion that the effect of π-π interaction overwhelms the effect of electrostatic repulsion. Therefore, electrostatic interaction is not the most important in governing the adsorption capacity.

In summary, the adsorption capacity of ACs on GO is mainly guided by the intensity of π-π interaction, with hydrophobic interaction, GO-ACs H-bond, vdWs attraction, and electrostatic interaction provides additional driving forces. Recent experimental studies also evidenced that the adsorption of ACs on GO was highly dependent on the π-π interactions rather than hydrophobic effects. [16, 65] Nitrobenzene exhibited the second weakest π-stacking ability and possessed the highest adsorption capacity, which should be a combined mechanism of stronger hydrophobicity and zero - electrostatic repulsion.

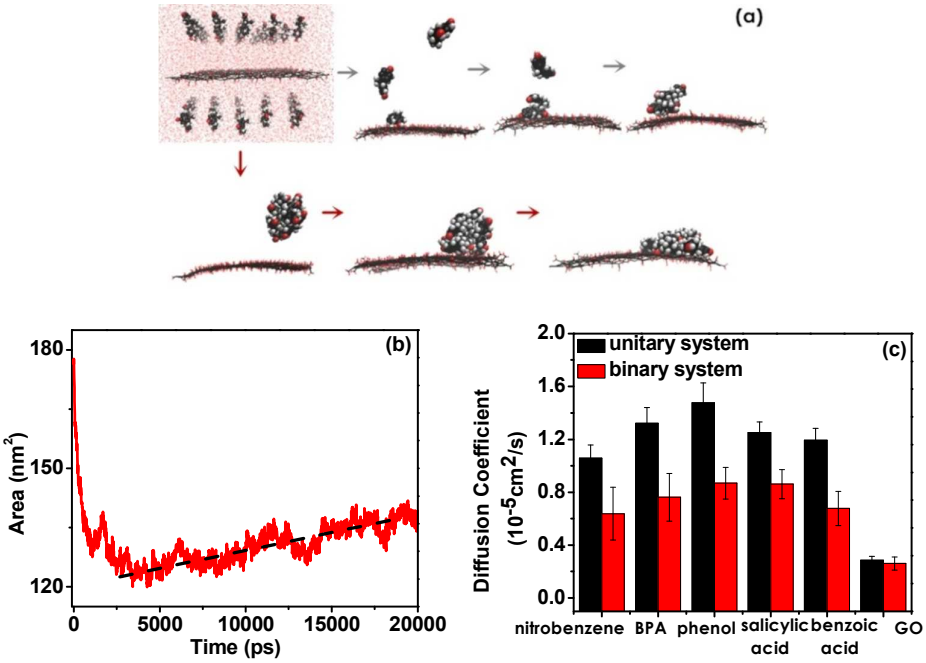

Fig. 6 (a) Two patterns for the multilayer adsorption. The grey arrows indicate the first pattern, and the red arrows indicate the self-aggregation-first pattern. (b) Evolution of the solvent accessible surface area of BPA during the adsorption. (c) Diffusion coefficients of GO and ACs.

Local Topology of ACs Adsorbed on GO

The configuration of individual AC molecules adsorbed on GO was reported extensively recently and an offset face-to-face π-π

stacking structure was proposed,[26-28] however, the effect of ACs concentrations was not incorporated. Considering that the local topology of ACs adsorbed on GO as a function of the ACs concentration will provide further understandings towards the interaction mechanism, MD simulations were performed.

Three model systems were built: 20 AC molecules were put into the 13×13×13 nm^3 water box to model the low concentration of ACs (system i), with 40 AC molecules (system ii) and 60 AC molecules (system iii) were put into the same water box to model the higher concentration of ACs. As shown in Fig. S8, at lower concentration (system i) where the adsorption sites are abundant, ACs adsorbed on GO mainly via monolayer absorption. ACs was lying down on the GO plane with offset face-to-face π-π interactions (Fig. S9(a)), consistent with our previous studies. [26-28] At higher concentrations, the adsorption configuration is related to the property of ACs. For phenol, even in system iii where 60 phenols were present, the main mechanism is monolayer adsorption (Fig. S9(b)); for BPA, the main adsorption mode is multi-layer adsorption (Fig. S9(c)). As illustrated in Fig. 6(a), two patterns were observed for the multi-layer adsorption by tracing the dynamic trajectories of BPA. One pattern is that BPAs adsorbed on GO via binding with the BPAs that have been adsorbed on GO (grey arrows in Fig. 6(a)). However, this is not the dominant pattern, and the multilayer adsorption is mainly accomplished via the first-self-aggregation mechanism (red arrows in Fig. 6(a)). Three stages are identified for this pattern: (I) significant aggregation of BPAs occurs before adsorbing on GO; (II) the BPA aggregates approach GO and bind with the GO in the form of multilayer adsorption; (III) the aggregates unfold to some extent and extend on the basal plane of GO, thus enhancing the binding with GO. The calculation of solvent accessible surface area (SASA) offers another measure to evaluate the evolution of BPA aggregates during the adsorption (Fig. 6(b)): self-aggregation of BPA is accompanied by a decrease of its SASA, and the unfolding of BPA aggregates upon adsorbing on GO is accompanied by a minor increase of its SASA.

The self-aggregation stage is crucial for the multilayer adsorption. For ACs with stronger hydrophilicity, self-aggregation is not favoured. More specifically, even in system iii where 60 phenols were present, only a few self-aggregations were observed, and phenols tended to adsorb on GO via monolayer adsorption. For BPA, the flexibility and the hydrophobic components facilitate its self-aggregation, and therefore, the multilayer adsorption is favourable for BPA even at lower concentration (Fig. S8).

According to the MD trajectories during the adsorption process, amount of ACs adsorbed on GO with time was obtained, and adsorption kinetics was predicted. The parameters (Table S6) indicated that the adsorption of ACs on GO can be satisfactorily fitted by the pseudo-first-order model, consistent with the experimental results (Table S7). However, deviations exist for the detailed parameters, which may be caused by the differences of sizes or morphologies (wrinkle or groove) of GOs used in MD simulations and experiments.

Effect of Adsorption on the Fate of ACs and GO

To understand how the presence of GO (ACs) impacts the behaviour of ACs (GO) in water, unitary and binary model systems were employed. The unitary systems contain only ACs or GO in water, while ACs and GO are both present in the binary system. Diffusion coefficients of ACs and GO in the unitary and binary systems were calculated using MD and are collected in Fig. 6(c). In the presence of GO, the diffusion coefficients of ACs decreased significantly, implying the translational motion of ACs was considerably slowed down. This suggests that the GO may retard the migration of ACs in water. However, no obvious difference was detected for the diffusion of GO upon the binding of ACs. These results provide molecular level of evidence that by anchoring ACs on the surface of GO-related materials, the migration behaviour of ACs will be significantly changed; however, the presence of ACs in the aqueous environment will not affect the migration of GO. In the previous section, it has been established that the aggregates of BPA will be unfolded upon binding on GO, thus the ACs that are originally buried in the aggregated structure may be now accessible for aquatic organisms and may lead to an increase of its biotoxicity.

In previous studies, Lan et al. mimicked the hydrophobic surface by a carbon nanotube. [20] Inspired by this, GO can be employed to mimic the carbonaceous surfaces in aquatic environment. Chars from vegetation fires, charcoal produced for fuel and atmospheric soot particles are all carbonaceous materials which contain carbon skeleton and functional groups such as carboxyl and hydroxyl.[66] Based on the investigation for the interaction between GO and ACs, it is reasonably inferred that released intentionally or unintentionally into the aquatic environment, carbonaceous surfaces will contribute greatly to alter the transport and toxicity of ACs in water.

Conclusions

In this study, adsorption of BPA, nitrobenzene, phenol, benzoic acid, salicylic acid on GO were investigated. Isotherm analysis showed the adsorption capacity is nitrobenzene (263.24 mg/g) > BPA (224.32 mg/g) > phenol (56.56 mg/g) > salicylic acid (33.64 mg/g) > benzoic acid (21.27 mg/g). To explore the causative factors behind the distinct adsorption capacity, π-π, H-bonds, vdWs, electrostatic interaction, and hydrophobic effect were examined. π-stacking is the most important property in regulating the adsorption capacity. The order of hydrophobicity, polarizability, negative charges carried by of ACs, and GO-ACs H-bond interaction intensity correlated poorly with the order of adsorption capacity, implying that hydrophobic interaction, vdWs, electrostatic interaction, and GO-AC H-bond interactions are not important in regulating the adsorption capacity. The configurations of ACs adsorbed on GO were captured and were found to be related to the concentration and properties of ACs. The calculations of diffusion coefficient and solvent accessible surface area provided molecular level of evidence that the interaction with GO will retard the migration and increase the bio-accessibility of ACs, which may in turn affect their fate and toxicity. In addition, the LOLIPOP values of twenty common ACs are provided, which will help to compare the π-stacking ability between ACs and materials containing benzene rings.

Acknowledgements

This paper is supported by National Natural Science Foundation of China (Grant Nos. 51278147, 50808052, 51408162, and 71671050), HIT Environment and Ecology Innovation Special Funds (Grant No.

HSCJ201606), China Postdoctoral Science Special Foundation (Grant No. 2016T90303), State Key Laboratory of Urban Water Resource and Environment (Grant No. 2016DX02), and USDA-NIFA Hatch program (MAS 00475). Huan Tang also thanks the China Scholarship Council for support of her study at the University of Massachusetts, Amherst.

Notes and references

1. K. Mikołajewska, J. Stragierowicz and J. Gromadzinska, Bisphenol A–Application, sources of exposure and potential risks in infants, children and pregnant women, *International journal of occupational medicine and environmental health*, 2015.
2. R. F. Lane, C. D. Adams, S. J. Randtke and R. E. Carter, Chlorination and chloramination of bisphenol A, bisphenol F, and bisphenol A diglycidyl ether in drinking water, *Water research*, 2015, **79**, 68-78.
3. E. Carmona, V. Andreu and Y. Picó, Occurrence of acidic pharmaceuticals and personal care products in Turia River Basin: from waste to drinking water, *Sci Total Environ*, 2014, **484**, 53-63.
4. A. Manna and C. Amutha, Laccase–silica nanoparticle conjugates can efficiently reduce the early maturation risk due to BPA in female Oreochromis mossambicus and its toxic load from the contaminated effluent, *Environmental Science: Nano*, 2017.
5. J. Peretz, L. Vrooman, W. A. Ricke, P. A. Hunt, S. Ehrlich, R. Hauser, V. Padmanabhan, H. S. Taylor, S. H. Swan and C. A. VandeVoort, Bisphenol A and reproductive health: update of experimental and human evidence, 2007–2013, *Environ Health Persp*, 2014, **122**, 775.
6. Y. Dai, J. Yao, Y. Song, S. Wang and Y. Yuan, Enhanced adsorption and degradation of phenolic pollutants in water by carbon nanotube modified laccase-carrying electrospun fibrous membranes, *Environmental Science: Nano*, 2016, **3**, 857-868.
7. M. S. Wolff, S. L. Teitelbaum, K. McGovern, S. M. Pinney, G. C. Windham, M. Galvez, A. Pajak, M. Rybak, A. M. Calafat and L. H. Kushi, Environmental phenols and pubertal development in girls, *Environment international*, 2015, **84**, 174-180.
8. Z. Cai, A. D. Dwivedi, W.-N. Lee, X. Zhao, W. Liu, M. Sillanpää, D. Zhao, C.-H. Huang and J. Fu, Application of nanotechnologies for removing pharmaceutically active compounds from water: development and future trends, *Environmental Science: Nano*, 2018.
9. B. Pan, D. Lin, H. Mashayekhi and B. Xing, Adsorption and hysteresis of bisphenol A and 17α-ethinyl estradiol on carbon nanomaterials, *Environ Sci Technol*, 2008, **42**, 5480-5485.
10. X. Luo, F. Deng, L. Min, S. Luo, B. Guo, G. Zeng and C. Au, Facile one-step synthesis of inorganic-framework molecularly imprinted TiO2/WO3 nanocomposite and its molecular recognitive photocatalytic degradation of target contaminant, *Environ Sci Technol*, 2013, **47**, 7404-7412.
11. F. Duan, C. Chen, X. Zhao, Y. Yang, X. Liu and Y. Qin, Water-compatible surface molecularly imprinted polymers with synergy of bi-functional monomers for enhanced selective adsorption of bisphenol A from aqueous solution, *Environmental Science: Nano*, 2016, **3**, 213-222.
12. P. Shao, J. Tian, F. Yang, X. Duan, S. Gao, W. Shi, X. Luo, F. Cui, S. Luo and S. Wang, Identification and Regulation of Active Sites on Nanodiamonds: Establishing a Highly Efficient Catalytic System for Oxidation of Organic Contaminants, *Adv Funct Mater*, 2018.
13. L. Wang, D. Zhu, J. Chen, Y. Chen and W. Chen, Enhanced adsorption of aromatic chemicals on boron and nitrogen co-doped single-walled carbon nanotubes, *Environmental Science: Nano*, 2017, **4**, 558-564.
14. W. Sun, C. Wang, W. Pan, S. Li and B. Chen, Effects of natural minerals on the adsorption of 17β-estradiol and bisphenol A on graphene oxide and reduced graphene oxide, *Environmental Science: Nano*, 2017.
15. T. Hüffer, H. Sun, J. D. Kubicki, T. Hofmann and M. Kah, Interactions between aromatic hydrocarbons and functionalized C 60 fullerenes–insights from experimental data and molecular modelling, *Environmental Science: Nano*, 2017, **4**, 1045-1053.
16. X. Chen and B. Chen, Macroscopic and spectroscopic investigations of the adsorption of nitroaromatic compounds on graphene oxide, reduced graphene oxide, and graphene nanosheets, *Environ Sci Technol*, 2015, **49**, 6181-6189.
17. J. Wang, B. Chen and B. Xing, Wrinkles and Folds of Activated Graphene Nanosheets as Fast and Efficient Adsorptive Sites for Hydrophobic Organic Contaminants, *Environ Sci Technol*, 2016, **50**, 3798-3808.
18. J. Wang, Z. Chen and B. Chen, Adsorption of polycyclic aromatic hydrocarbons by graphene and graphene oxide nanosheets, *Environ Sci Technol*, 2014, **48**, 4817-4825.
19. H. Dong, W. Gao, F. Yan, H. Ji and H. Ju, Fluorescence resonance energy transfer between quantum dots and graphene oxide for sensing biomolecules, *Anal Chem*, 2010, **82**, 5511-5517.
20. J. Balapanuru, J. X. Yang, S. Xiao, Q. Bao, M. Jahan, L. Polavarapu, J. Wei, Q. H. Xu and K. P. Loh, A Graphene Oxide–Organic Dye Ionic Complex with DNA-Sensing and Optical-Limiting Properties, *Angewandte Chemie*, 2010, **122**, 6699-6703.
21. X. Liu, R. Aizen, R. Freeman, O. Yehezkeli and I. Willner, Multiplexed aptasensors and amplified DNA sensors using functionalized graphene oxide: application for logic gate operations, *ACS nano*, 2012, **6**, 3553-3563.
22. M. Chen, G. Zeng, P. Xu, Y. Zhang, D. Jiang and S. Zhou, Understanding enzymatic degradation of single-walled carbon nanotubes triggered by functionalization using molecular dynamics simulation, *Environmental Science: Nano*, 2017, **4**, 720-727.
23. Z. Luo, S. Li, Y. Xu, H. Ren, X. Zhang, G. Hu, F. Huang and T. Yue, Extracting pulmonary surfactants to form inverse micelles on suspended graphene nanosheets, *Environmental Science: Nano*, 2018.
24. H. Tang, Y. Zhao, S. Shan, X. Yang, D. Liu, F. Cui and B. Xing, Wrinkle- and Edge-Adsorption of Aromatic

Compounds on Graphene Oxide as Revealed by Atomic Force Microscopy, Molecular Dynamics Simulation, and Density Functional Theory, *Environmental Science & Technology*, 2018, **52**, 7689-7697.

25. X. Chen, S. Jia, N. Ding, J. Shi and Z. Wang, Capture of aromatic organic pollutants by hexagonal boron nitride nanosheets: density functional theoretical and molecular dynamic investigation, *Environmental Science: Nano*, 2016, **3**, 1493-1503.
26. H. Tang, Y. Zhao, X. Yang, D. Liu, S. Shan, F. Cui and B. Xing, Understanding the pH-dependent adsorption of ionizable compounds on graphene oxide using molecular dynamics simulations, *Environmental Science: Nano*, 2017, **4**, 1935-1943.
27. S. Yu, X. Wang, W. Yao, J. Wang, Y. Ji, Y. Ai, A. Alsaedi, T. Hayat and X. Wang, Macroscopic, spectroscopic, and theoretical investigation for the interaction of phenol and naphthol on reduced graphene oxide, *Environ Sci Technol*, 2017, **51**, 3278-3286.
28. Z. Jin, X. Wang, Y. Sun, Y. Ai and X. Wang, Adsorption of 4-n-nonylphenol and bisphenol-A on magnetic reduced graphene oxides: a combined experimental and theoretical studies, *Environ Sci Technol*, 2015, **49**, 9168-9175.
29. S. Yu, X. Wang, Y. Ai, X. Tan, T. Hayat, W. Hu and X. Wang, Experimental and theoretical studies on competitive adsorption of aromatic compounds on reduced graphene oxides, *J Mater Chem A*, 2016, **4**, 5654-5662.
30. W. Song, T. Yang, X. Wang, Y. Sun, Y. Ai, G. Sheng, T. Hayat and X. Wang, Experimental and theoretical evidence for competitive interactions of tetracycline and sulfamethazine with reduced graphene oxides, *Environmental Science: Nano*, 2016, **3**, 1318-1326.
31. N. I. Kovtyukhova, P. J. Ollivier, B. R. Martin, T. E. Mallouk, S. A. Chizhik, E. V. Buzaneva and A. D. Gorchinskiy, Layer-by-layer assembly of ultrathin composite films from micron-sized graphite oxide sheets and polycations, *Chem Mater*, 1999, **11**, 771-778.
32. H. Tang, Y. Zhao, X. Yang, D. Liu, P. Shao, Z. Zhu, S. Shan, F. Cui and B. Xing, New Insight into the Aggregation of Graphene Oxide Using Molecular Dynamics Simulations and Extended Derjaguin–Landau–Verwey–Overbeek Theory, *Environ Sci Technol*, 2017, **51**, 9674-9682.
33. X. Hu, W. Kang and L. Mu, Aqueously Released Graphene Oxide Embedded in Epoxy Resin Exhibits Different Characteristics and Phytotoxicity of Chlorella vulgaris from the Pristine Form, *Environ Sci Technol*, 2017.
34. C. Tian, J. Zhao, J. Zhang, S. Chu, Z. Dang, Z. Lin and B. Xing, Enhanced removal of roxarsone by Fe 3 O 4@ 3D graphene nanocomposites: synergistic adsorption and mechanism, *Environmental Science: Nano*, 2017, **4**, 2134-2143.
35. S. Yu, X. Wang, Y. Ai, Y. Liang, Y. Ji, J. Li, T. Hayat, A. Alsaedi and X. Wang, Spectroscopic and theoretical studies on the counterion effect of Cu (II) ion and graphene oxide interaction with titanium dioxide, *Environmental Science: Nano*, 2016, **3**, 1361-1368.
36. A. Lerf, H. He, M. Forster and J. Klinowski, Structure of graphite oxide revisited, *The Journal of Physical Chemistry B*, 1998, **102**, 4477-4482.
37. L. Wang, K. Lee, Y.-Y. Sun, M. Lucking, Z. Chen, J. J. Zhao and S. B. Zhang, Graphene oxide as an ideal substrate for hydrogen storage, *ACS nano*, 2009, **3**, 2995-3000.
38. I. Chowdhury, M. C. Duch, N. D. Mansukhani, M. C. Hersam and D. Bouchard, Colloidal properties and stability of graphene oxide nanomaterials in the aquatic environment, *Environmental science & technology*, 2013, **47**, 6288-6296.
39. H. Tang, D. Liu, Y. Zhao, X. Yang, J. Lu and F. Cui, Molecular dynamics study of the aggregation process of graphene oxide in water, *The Journal of Physical Chemistry C*, 2015, **119**, 26712-26718.
40. H. Tang, Y. Zhao, X. Yang, D. Liu, S. Shan and F. Cui, Understanding the Roles of Solution Chemistries and Functionalization on the Aggregation of Graphene-Based Nanomaterials Using Molecular Dynamic Simulations, *J Phys Chem C*, 2017.
41. N. Wei, C. Lv and Z. Xu, Wetting of graphene oxide: a molecular dynamics study, *Langmuir*, 2014, **30**, 3572-3578.
42. W. L. Jorgensen, D. S. Maxwell and J. Tirado-Rives, Development and testing of the OPLS all-atom force field on conformational energetics and properties of organic liquids, *J Am Chem Soc*, 1996, **118**, 11225-11236.
43. D. Van Der Spoel, E. Lindahl, B. Hess, G. Groenhof, A. E. Mark and H. J. Berendsen, GROMACS: fast, flexible, and free, *J Comput Chem*, 2005, **26**, 1701-1718.
44. H. Berendsen, J. Grigera and T. Straatsma, The missing term in effective pair potentials, *Journal of Physical Chemistry*, 1987, **91**, 6269-6271.
45. B. Hess, H. Bekker, H. J. Berendsen and J. G. Fraaije, LINCS: a linear constraint solver for molecular simulations, *J Comput Chem*, 1997, **18**, 1463-1472.
46. M. S. K. P. SETTLE, An analytical version of the SHAKE and RATTLE algorithm for rigid water molecules, *J. Comput. Chem*, 1992, **13**, 952-962.
47. A. Lemak and N. Balabaev, On the Berendsen thermostat, *Molecular Simulation*, 1994, **13**, 177-187.
48. A. Luzar and D. Chandler, Hydrogen-bond kinetics in liquid water, *Nature*, 1996, **379**, 55-57.
49. M. Chen, X. Lu, X. Liu, Q. Hou, Y. Zhu and H. Zhou, Retardation of Water Reorientation at the Oil/Water Interface, *J Phys Chem C*, 2015, **119**, 16639-16648.
50. M. Frisch, G. Trucks, H. Schlegel, G. Scuseria, M. Robb, J. Cheeseman, G. Scalmani, V. Barone, B. Mennucci and G. Petersson, Gaussian 09, revision D. 01.*Journal*, 2009.
51. L. Turi and J. Dannenberg, Correcting for basis set superposition error in aggregates containing more than two molecules: ambiguities in the calculation of the counterpoise correction, *The Journal of Physical Chemistry*, 1993, **97**, 2488-2490.
52. T. Lu and F. Chen, Multiwfn: a multifunctional wavefunction analyzer, *J Comput Chem*, 2012, **33**, 580-592.
53. K. Yang, B. Chen, X. Zhu and B. Xing, Aggregation, adsorption, and morphological transformation of graphene oxide in aqueous solutions containing

different metal cations, *Environmental science & technology*, 2016, **50**, 11066-11075.
54. S. Zinadini, A. A. Zinatizadeh, M. Rahimi, V. Vatanpour and H. Zangeneh, Preparation of a novel antifouling mixed matrix PES membrane by embedding graphene oxide nanoplates, *J Membrane Sci*, 2014, **453**, 292-301.
55. C. T. Jafvert and P. P. Kulkarni, Buckminsterfullerene's (C60) octanol− water partition coefficient (K ow) and aqueous solubility, *Environ Sci Technol*, 2008, **42**, 5945-5950.
56. G. Ersan, Y. Kaya, O. G. Apul and T. Karanfil, Adsorption of organic contaminants by graphene nanosheets, carbon nanotubes and granular activated carbons under natural organic matter preloading conditions, *Sci Total Environ*, 2016, **565**, 811-817.
57. S.-W. Nam, C. Jung, H. Li, M. Yu, J. R. Flora, L. K. Boateng, N. Her, K.-D. Zoh and Y. Yoon, Adsorption characteristics of diclofenac and sulfamethoxazole to graphene oxide in aqueous solution, *Chemosphere*, 2015, **136**, 20-26.
58. G. A. Jeffrey and G. A. Jeffrey, *An introduction to hydrogen bonding*, Oxford university press New York, 1997.
59. Y. Jiang, R. Raliya, P. Liao, P. Biswas and J. Fortner, Graphene Oxides in Water: Assessing Stability as a Function of Material and Natural Organic Matter Properties, *Environmental Science: Nano*, 2017.
60. J. W. Bloom and S. E. Wheeler, Taking the aromaticity out of aromatic interactions, *Angew Chem Int Edit*, 2011, **50**, 7847-7849.
61. Y. Zhou, O. G. Apul and T. Karanfil, Adsorption of halogenated aliphatic contaminants by graphene nanomaterials, *Water research*, 2015, **79**, 57-67.
62. B. Konkena and S. Vasudevan, Understanding aqueous dispersibility of graphene oxide and reduced graphene oxide through p K a measurements, *The journal of physical chemistry letters*, 2012, **3**, 867-872.
63. I. Raskin, Role of salicylic acid in plants, *Annual review of plant biology*, 1992, **43**, 439-463.
64. S. Chou and C. Huang, Application of a supported iron oxyhydroxide catalyst in oxidation of benzoic acid by hydrogen peroxide, *Chemosphere*, 1999, **38**, 2719-2731.
65. L. Ji, W. Chen, Z. Xu, S. Zheng and D. Zhu, Graphene nanosheets and graphite oxide as promising adsorbents for removal of organic contaminants from aqueous solution, *Journal of environmental quality*, 2013, **42**, 191-198.
66. J. J. Pignatello, Interactions of anthropogenic organic chemicals with natural organic matter and black carbon in environmental particles, *Biophysico-chemical processes of anthropogenic organic compounds in environmental systems*, 2011, 1-50.

Two patterns for the multilayer adsorption